B-RAD: a radiation survey meter for operation in intense magnetic fields

Published by IOP Publishing for Sissa Medialab

Received: *November 13, 2018*
Revised: *March 27, 2019*
Accepted: *May 10, 2019*
Published: *May 28, 2019*

TECHNICAL REPORT

2019 JINST 14 T05007

B-RAD: a radiation survey meter for operation in intense magnetic fields

D. Celeste,[a,1] **A. Curioni,**[a] **A. Fazzi,**[b] **M. Silari**[a] **and V. Varoli**[b]

[a] *CERN, Geneva 23, 1211 Switzerland*
[b] *Politecnico of Milano, Via La Masa 34, Milano, 20156 Italy*

E-mail: damiano.celeste@cern.ch

Abstract: B-RAD is a hand-held radiation survey meter, specifically designed for operation in regions of strong magnetic field. The instrument has been jointly developed by CERN Radiation Protection group and the Department of Energy of the Polytechnic of Milan (POLIMI), originally to perform measurements of the residual radioactivity (radiation surveys) in the experimental areas of CERN Large Hadron Collider (LHC) and inside the ATLAS detector without switching the magnetic field off. B-RAD is based on a scintillating crystal coupled to Silicon Photomultipliers, and its operation is unaffected by magnetic field intensity up to 3 T. Five engineered prototype units were built and made available for routine use at CERN. The design of the instrument has subsequently been licenced to a company in order to industrialise it. This paper describes the CERN-POLIMI engineered version of the instrument, discusses its characterization in details and provides an overview of the commercial unit.

Keywords: Gamma detectors (scintillators, CZT, HPG, HgI etc); Radiation monitoring; Scintillators, scintillation and light emission processes (solid, gas and liquid scintillators); Photon detectors for UV, visible and IR photons (solid-state) (PIN diodes, APDs, Si-PMTs, G-APDs, CCDs, EBCCDs, EMCCDs, CMOS imagers, etc)

[1]Corresponding author.

https://doi.org/10.1088/1748-0221/14/05/T05007

Contents

2019 JINST 14 T05007

1 Introduction

The request for a radiation survey meter able to operate reliably inside a strong magnetic field came from CERN LHC experiments [1], based on the requirement of carrying out measurements of residual radioactivity in the underground experimental areas without switching off the intense magnetic field of the detectors. Operational measurements in the presence of magnetic fields up to 1 T have to be performed in different locations in the experimental halls and inside the accessible areas of the ATLAS detector. The most immediate need is for surveys of gamma radiation. First tests on commercial devices with minimum needed requirements (MiniAlarm (ThermoScientific), Teletector (Automess), FH40 (ThermoScientific), AD6 (Automess), Victoreen (Fluke), DMC 2000 XB (MirionTechnologies), DMC 2000 S (MirionTechnologies), SOR/R and SOR/T (LaurusSystems)) able to detect radiation, measure dose rate and integrated dose (RADOS DIS1) were performed by the CERN Radiation Protection group between 2009 and 2010. All of the tested devices available at that time failed in the presence of rather weak magnetic fields below 0.3 T, and several of them showed deficiencies already at 0.1 T. The development of B-RAD started in 2010, through a collaboration between CERN RP group and the Polytechnic of Milan (POLIMI). The development of this instrument, due to the peculiarity of the project and the complexity of a multilateral collaboration, took several years before achieving the goal of a final commercial version. Nowadays, thanks to novel technologies, new devices are commercialized

by various manufacturers. Taking as a reference a public document from the U.S. Department of Homeland security [2] published in July 2017, only four out of twenty-three devices guarantee our minimum requirements in terms of a detection technology insensitive to magnetic field (up to 1 T), dose rate range (0.1 μSv/h to few mSv/h), energy threshold (60 keV) and energy range (up to 1.4 MeV). Concerning these four devices (Smartshield G300 by Passport Systems, GammaRAE II R by Rae Systems, RadPavise by X-Z Lab and Identifinder R300 by FLIR Detection) more accurate information on the electronics are needed to verify the presence of any component sensitive to magnetic field, e.g. inductive elements. Battery drain/heating or LCD screen failure tests need to be performed to certify the complete magnetic field insensitivity of the instrument. Last, but not least, any ferromagnetic material (such as shells, screws and frames) should have been avoided in the development of these devices to make them operational in the presence of magnetic field. Not only the employed detection technology, but the whole electronic and mechanical assembly is crucial to reach this goal. The B-RAD consists of an active probe equipped with a scintillating crystal coupled to an array of Silicon Photomultipliers (SiPM), connected through a cable to a control unit, which houses batteries, a microcontroller, various magnetic field insensitive electronic circuitry and displays. Since the average energy of gamma rays from residual radioactivity in particle accelerator facilities is around 800 keV [3], B-RAD was designed to cover the energy range for gamma rays between 60 keV (^{241}Am photons) and 1.3 MeV (^{60}Co photons). The sensitivity range, in terms of dose rate for gamma radiation, was initially set between 1 μSv/h and a few mSv/h. By changing the size of the crystal, this range was later extended, with a lower limit down to 0.1 μSv/h, i.e. ambient background. After the first prototype was confirmed to operate correctly in magnetic field, five engineered units were built, tested in magnetic field up to 3 T and then made available for routine use with CERN RP group. The instrument has been jointly patented by CERN and POLIMI [4]. CERN has subsequently licensed the B-RAD design to the company ELSE NUCLEAR [5], which has produced an industrial version of the instrument, provided with a probe for both dose rate and gamma-spectrometry measurements, which has just been made available commercially.

This paper discusses the design of the engineered version of B-RAD (control unit and probe), the choice of the crystal, the performance tests in magnetic field, the linearity of its response, the dependence on temperature and the solution adopted for its compensation, energy response and approach used to flatten it, the spectrometric performance. A short account of the upgrades made by the company for the industrialised version is also given.

2 Description of the instrument

The instrument consists of two parts: an active probe and a control unit, connected through a cable. A picture of the two parts (the probe has the front cover removed to show the crystal) is shown in figure 1.

$LaBr_3$(Ce) was chosen as the scintillating crystal in virtue of its fast decay time (16 ns), high density (5.06 g/cm^3) and high light yield of 63 photons per keV of deposited energy [6]. The fast response of $LaBr_3$(Ce) is crucial in handling the high count rate (several hundred thousand counts per second) encountered in typical applications in radiation protection. Moreover, $LaBr_3$(Ce) has a good temperature stability (see section 3.3) and — among scintillating crystals — it offers an excellent intrinsic energy resolution, slightly above 3% FWHM at 662 keV [7], which is interesting

2019 JINST 14 T05007

Figure 1. B-RAD. On the left, the probe with the front cover removed. The cylindrical case of the scintillating crystal is visible, sitting on the board housing the SiPM. On the right, the front panel of the control unit. The ON/OFF rotary switch, the Start/Stop button, the LED indicators for the battery status, the LED display (showing "CERN") and the liquid crystal display can be seen.

in view of the final application of the commercial instrument as a hand-held gamma spectrometer. The size of the scintillating crystal was dictated by the required sensitivity range. Three of the engineered units are equipped with a crystal in the shape of a rectangular cuboid ($4 \times 4 \times 15\,mm^3$) and two with cylindrical crystals. One of the latter has 10 mm diameter and 10 mm height ($10\,\emptyset \times 10\,mm^3$), while one unit has been equipped with a larger 1 inch (25.4 mm) right cylindrical crystal ($25.4\,\emptyset \times 25.4\,mm^3$), in order to extend the sensitivity down to lower dose rates (see table 1). In this last case, both NaI(Tl) and $LaBr_3$(Ce) crystals were tested. Additional tests were performed using a cylindrical $15\,\emptyset \times 15\,mm^3$ $LaBr_3$(Ce) crystal, which best matches the size of the SiPM array finally chosen and offers the best compromise between sensitivity at the low end of the dose rate range (ambient background) and manageable counting rate for dose rates exceeding 1 mSv/h. Figure 2 provides a schematic view of the main functions of the instrument.

Table 1. Main features of the five engineered units of B-RAD.

UNIT	CRYSTAL SHAPE	CRYSTAL DIMENSIONS	CRYSTAL MATERIAL	SiPM MODULE (ST Microelectronics)
Unit 1	Rectangular	$4 \times 4 \times 15\,mm^3$	$LaBr_3$(Ce)	1 element, $4 \times 4\,mm^2$
Unit 2	Rectangular	$4 \times 4 \times 15\,mm^3$	$LaBr_3$(Ce)	1 element, $4 \times 4\,mm^2$
Unit 3	Cylindrical	$10\,\emptyset \times 10\,mm^3$	$LaBr_3$(Ce)	4 elements, $4 \times 4\,mm^2$
Unit 4	Cylindrical	$25.4\,\emptyset \times 25.4\,mm^3$	NaI(Tl)/$LaBr_3$(Ce)	16 elements, $4 \times 4\,mm^2$
Unit 5	Rectangular	$4 \times 4 \times 15\,mm^3$	$LaBr_3$(Ce)	1 element, $4 \times 4\,mm^2$

2.1 Control unit

The control unit is enclosed in a plastic box, which can be fastened at the operator's waist. It consists of a counter with two displays (a primary LCD display and a LED screen in case of display

2019 JINST 14 T05007

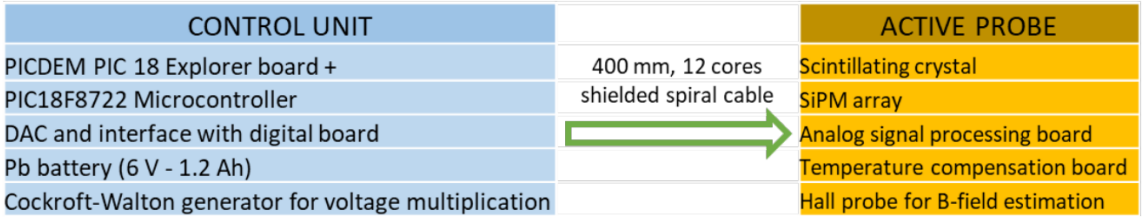

Figure 2. Main functions of the control unit and of the active probe.

failure), USB data interface, detector power supply board and battery with recharger circuit. The control unit is connected to the probe with a 400 mm shielded 12 cores (SPIRAFLEX PUR-CY SP-DSR-014) spiral cable for power supply and signal transmission. The dimensions of the control unit are 22.5 cm × 19.9 cm × 7.3 cm (h), the dimensions of the probe are 16.4 cm × 10.8 cm × 4.2 (h), their weights are 1.272 kg and 0.584 kg, respectively.

The digital board is a PICDEM PIC18 Explorer board (Microchip Technology) [8]. Although this demonstrator board is not optimized for integration in a compact instrument, and actually dictates the overall size of the control unit, it was selected because it is particularly handy during a development phase. Among other things, this board contains one microcontroller, one liquid crystal display (LCD), 9 LEDs, input/output ports, USB and RS-232 I/O connections, 2 push buttons. This board offers the possibility to select two different microcontrollers (PIC18F8722 or PIC18F87J11). In B-RAD only the main microcontroller of the board is used (PIC18F8722).

There exist two versions of the firmware to drive the microcontroller unit, one written using the Assembler language and one written in C language: in both cases the firmware manages the count rate and count integration, the count rate to dose rate conversion, all display functionalities and battery level information, as well as software interactions. A software interface written in BASIC language was developed to connect the instrument to a personal computer via USB, allowing to remotely start/stop the instrument, to perform calibration measurements (in units of counts per second), to set parameters as the bias voltage of the SiPM and calibration factors, and to transfer data to the hard disk of a computer for storage and offline analysis.

The battery is a rechargeable Pb battery (6 V, 1.200 mA · h); the circuitry to charge the battery is housed in the control unit, with a chip that allows charging the battery when connected and prevents the battery drift if disconnected. The charge level of the battery is shown both on a nine LEDs scale on the front panel and on the LCD display. The average power consumption during operation is 0.13 A at 6 V; therefore the battery life in continuous operation easily exceeds four hours. It takes about two hours to recharge the battery after a full discharge. In view of further developments, tests were performed with a higher capacity Li-ion rechargeable battery (H2B297 from HY-LINE, 7.4 V, 4.600 mA · h), showing a reliable performance in magnetic fields up to 1 T, through several charging and discharging cycles. Battery performances in the commercial version improved, after optimization, to reach more than 8 hours of continuous operation (see section 5).

The bias voltage for the SiPMs is generated inside the control unit and is fed to the SiPM array through the connecting cable. It is obtained by multiplying the 6 V supplied by the Pb battery with a ×6 [times six] Cockcroft-Walton generator and a switch controlled by the clock, which generates a 0–6 V signal. This method gives 36 V, used to feed the SiPM array through a voltage regulator,

2019 JINST 14 T05007

without using any inductive element, which would fail in the presence of a magnetic field. A digital-to-analog converter (DAC), controlled by the microcontroller and software, is used to set the correct bias voltage for the photo-detector on the voltage regulator output.

2.2 Active probe

The active probe is housed inside a light aluminum box provided with a handle. The active element is a scintillating crystal (see table 1), coupled to a Silicon Photomultiplier (SiPM) or arrays of SiPMs (depending on the size of the crystal). The amplifier and discrimination circuits and the power supply regulator board are housed in the same box.

For the five engineered units, prototype SiPMs from STMicroelectronics [9] were used. These SiPM are not commercially available and were characterised in the Nuclear Electronics Laboratory of POLIMI. Their Breakdown Voltage V_{BD} was estimated to be approximately 28 V. For the subsequent developments, commercially available SiPM arrays from SensL [10] were tested, with completely satisfactory results.

The pixel area of the ST Microelectronics SiPM is 4×4 mm^2, with 3600 microcells. The SiPMs have a plastic resin micro-packaging that protects the silicon chip and allows good optical coupling with the crystals. Various configurations of SiPM arrays were tried for the probes, according to the different sizes of the crystals. A 2×2 SiPM array was used for Unit 3 coupled to the cylindrical crystal of 10 mm diameter. In this case, the bias voltage is sent to the SiPM through a 30 pin connector and filtered, while the signals from the photo-detector are split into two lines (Fast and Slow) and sent to the main board of the active probe for signal processing. For the smallest crystals, with base of 4×4 mm^2 area, a single SiPM pixel is used (Units 1, 2 and 5). For reading the 1 inch cylindrical crystal in Unit 4, a matrix of 4×4 SiPMs is used.

A system allowing to exploit either a fast or a slow signal is implemented on the main board of the active probe. The fast signal solution is in particular well suited for high rate applications. In this configuration the signal from the SiPM is filtered through a C-R network, which reduces the slow components of the signal. The pulses are amplified and then sent to a shaping stage in order to obtain proper signals to be processed by an ADC and a comparator (MAX9203) for counting, and to be sent to the main board unit for acquisition. The comparator is AC-coupled to reject offsets and offset drifts. The comparator threshold is obtained by implementing a fixed and not modifiable reference voltage circuit in order to stabilize the voltage level as much as possible on the hardware. The threshold calibration is then performed via software by sweeping the bias voltage of the SiPM down to the right level allowing to measure 60 keV photons from ^{241}Am. This board also supplies the correct bias voltage to the SiPM array through a voltage regulator, which receives the 36 V as input and generates the bias according to the DAC instructions. A simplified block diagram of the instrument describing the signal processing is presented in figure 3. Concerning the voltage multiplication shown in figure 4, we exploit here the battery DC 6 V combined to the microcontroller clock output through a voltage inverter (SNAC04 [11]) and two MOSFETs (p-channel and n-channel in Si4532 [12]). This architecture allows to obtain a 0–6 V square wave as an input to the Cockcroft-Walton multiplier with the same frequency as the clock (input C1 capacitor). As known from ref. [13], the following six capacitor/diode networks are used to rectify and multiply the voltage input at each stage. In this way, we are able to obtain a DC output six times higher than the battery voltage (i.e. 36 V). The Cockcroft-Walton multiplier output is sent from the control unit

2019 JINST 14 T05007

to the active probe in figure 5 as an input to the voltage regulator TPS7A4001 [14]. The resulting voltage output (i.e. the SiPM bias voltage) varies following the voltage level at R8 which depends on the contributions of the temperature sensor (section 3.3) and the DAC. We are able to sweep the bias by modifying the DAC value through the microcontroller and to regulate it as a function of the temperature. This electronic architecture always keeps all different contributions decoupled one from the other [15].

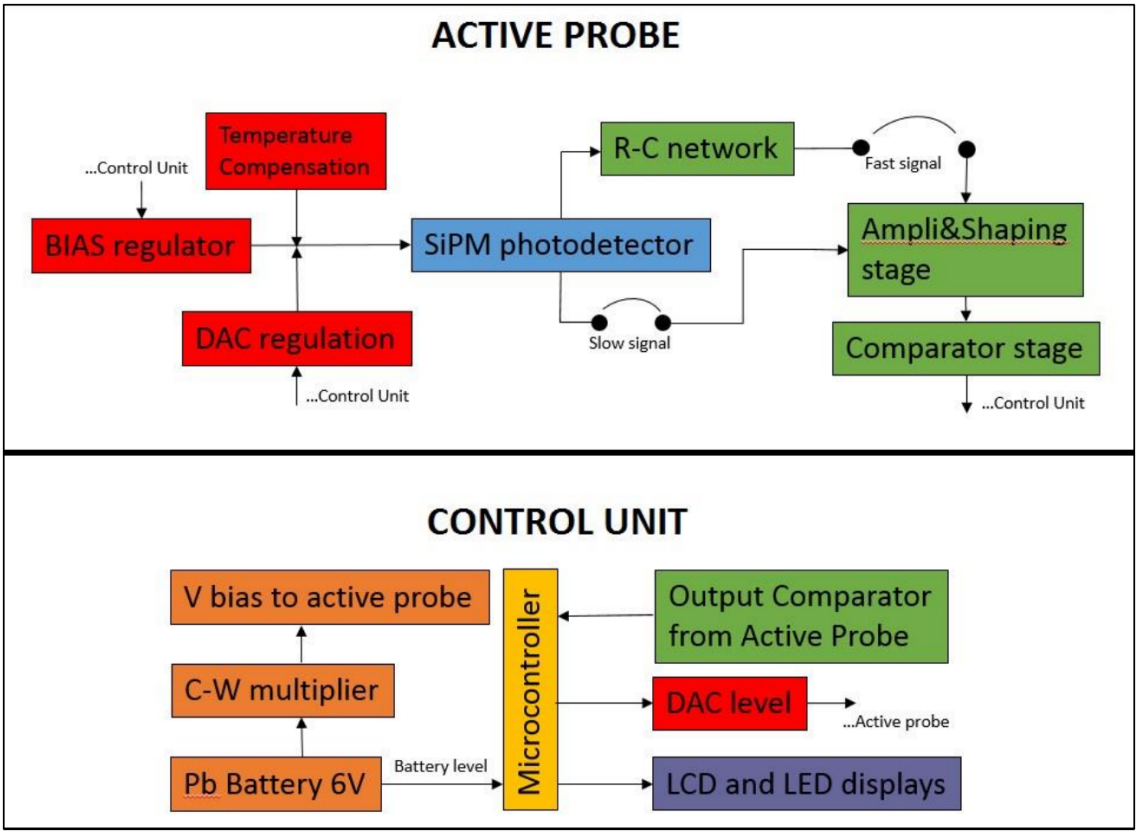

Figure 3. Block diagram of active probe and control unit. The Cockroft-Walton voltage multiplier and the red blocks in the active probe are shown in figure 4 and figure 5.

3 Performance tests of the instrument

This section discusses measurements performed on the prototype and the five engineered versions of the instrument. In particular, we focused on the response linearity in the dose rate range between 1 µSv/h and 10 mSv/h, on the insensitivity to the magnetic field up to 3 T and on the effect of the temperature variation (from −20°C to + 50°C) on the system.

3.1 Dose rate measurements

The B-RAD has been characterized extensively in terms of dose rate response, which is the primary purpose of a survey meter. Most measurements were performed at the energy of ^{137}Cs at the CERN RP calibration facility [16]. This laboratory, which is used to calibrate all CERN RP

2019 JINST 14 T05007

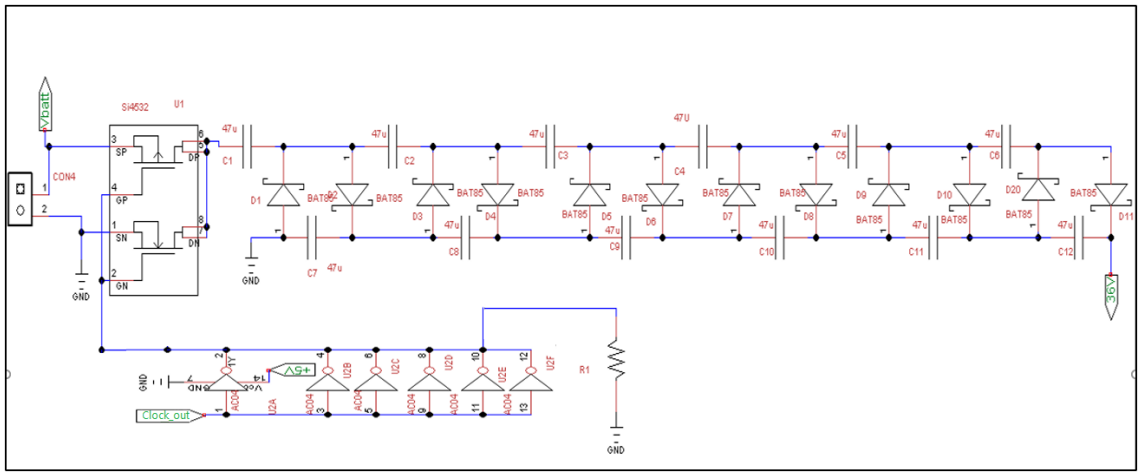

Figure 4. Cockcroft-Walton voltage multiplier schematic.

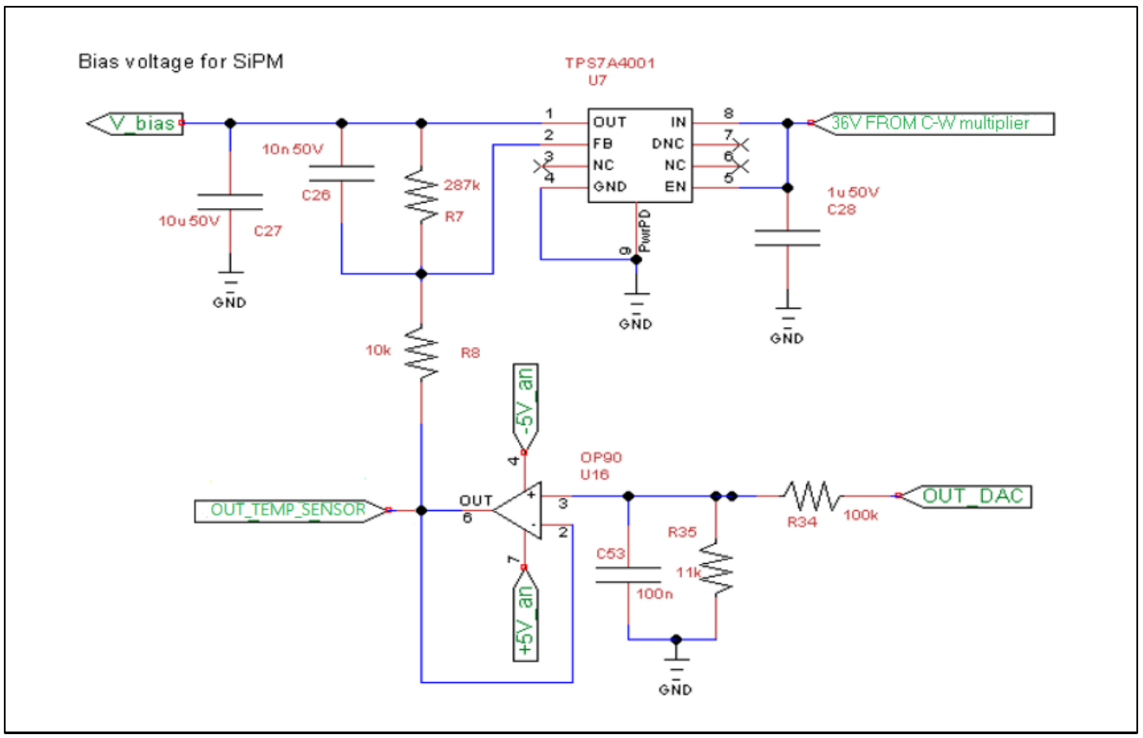

Figure 5. Electronic schematic of the bias voltage system.

instrumentation (personal dosimeters, hand-held survey meters and fixed monitors), is equipped with several calibrated radioactive sources and a motorized test bench, allowing to perform very precise dose rate measurements. The dose rate can be adjusted by changing the distance of the instrument from the source. The bench is provided with a 5 m rail that can be remotely controlled from the control room with a half-millimeter precision; the instrument is aligned by two lasers and placed with the active probe facing the irradiator. The distance from the source and the source activity were chosen to obtain specified values of dose rate. Figure 6 shows the response in terms of counts per second (cps) versus dose rate for the five units.

2019 JINST 14 T05007

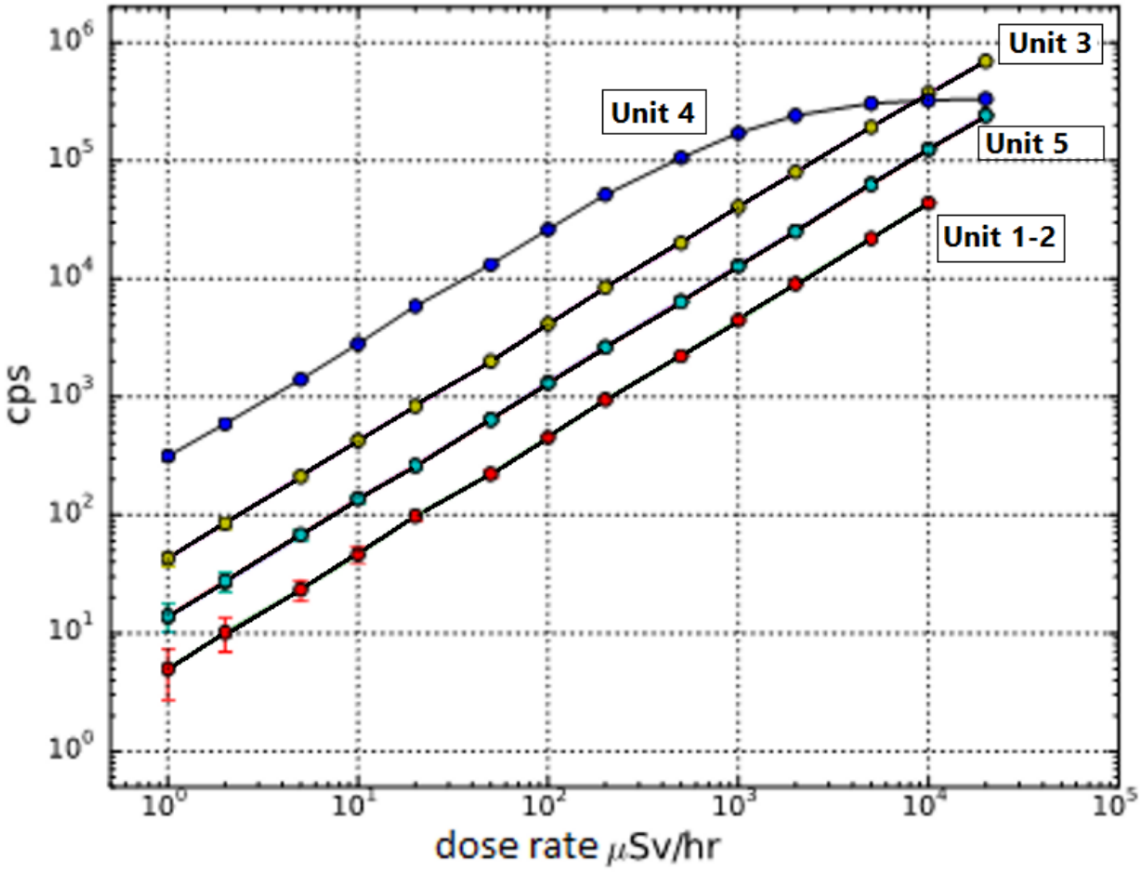

Figure 6. Count rate (counts per second, cps) versus dose rate linearity measurements on the five units. Units 1 and 2 equipped with a $4 \times 4 \times 15\,\mathrm{mm}^3$ $LaBr_3$ crystal overlap (red dots), Unit 5 (green dots) mounts the same crystal as Units 1 and 2 but has a lower energy threshold, Unit 3 (yellow dots) mounts a cylindrical $10\,\emptyset \times 10\,\mathrm{mm}^3$ $LaBr_3$ crystal, Unit 4 (blue dots) mounts a cylindrical $25.4\,\emptyset \times 25.4\,\mathrm{mm}^3$ NaI crystal.

All of the units were set and calibrated to have a lower energy threshold of 60 keV, except for Unit 5 which was tested with an energy threshold of 50 keV to check any influence of the choice of the threshold. Except for the higher count rate of Unit 5 as compared to Units 1 and 2, no remarkable differences is noticed. The response of all units mounting $LaBr_3$ crystals is linear up to 10 mSv/h, beyond our basic requirements, while Unit 4 mounting a NaI crystal shows a much faster saturation due to the decay time of the scintillating signal and starts deviating from linearity above about 1 mSv/h.

Figure 7 shows the cps to dose rate calibration factor for Unit 5. The measurements were performed using three different radioactive sources (^{137}Cs, ^{241}Am, ^{60}Co), even if only the ^{137}Cs source was over the entire range of dose rate. The other two sources were calibrated in between 0.5 μSv/h and 20 μSv/h. These tests allowed estimating the calibration factor at three different photon energy values: 60 keV, 662 keV and 1.3 MeV. As expected, due to different detection efficiencies that are further analyzed in section 4.1, the count rate values decrease with increasing energy: 244 cps/μSv/h for ^{241}Am, 19 cps/μSv/h for ^{137}Cs and 10 cps/μSv/h for ^{60}Co.

2019 JINST 14 T05007

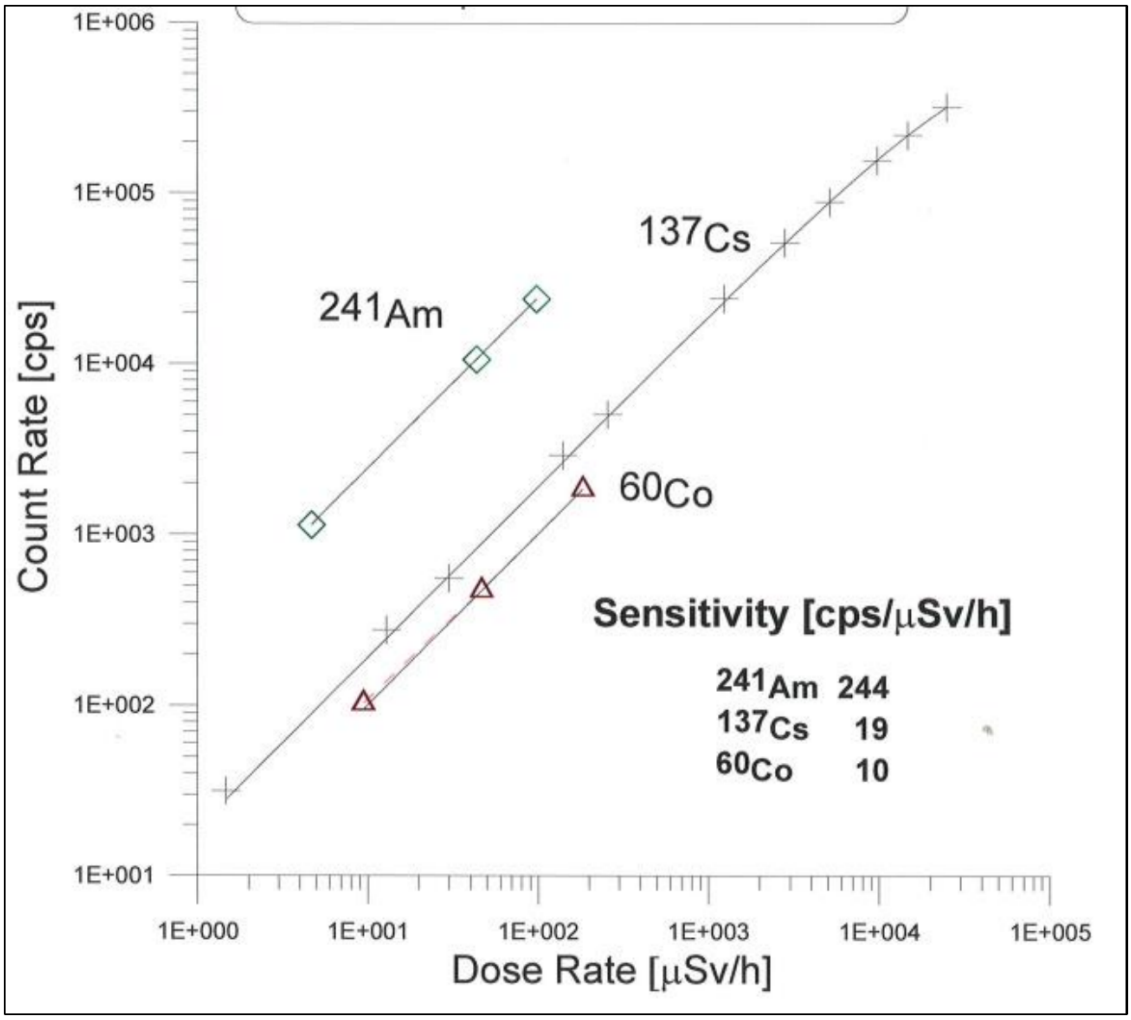

Figure 7. Cps to μSv/h calibration factors for Unit 5.

3.2 Tests in magnetic field

A number of tests to verify the insensitivity of the instrument to strong magnetic fields were carried out at CERN inside a calibrated dipole magnet. First, the electronic components were individually tested. The field was increased in 0.1 T steps up to 1 T and, during all measurements, no issues were remarked on the data acquisition or the battery life. Unlike the LCD display which started failing at 0.7 T, the LED display worked without any problem up to 1 T. Then, a test of the effect of the magnetic field on the actual dose measurement with the assembled probe prototype was performed with a ^{60}Co source with a contact dose rate of 2 mSv/h. The source was held in a fixed position with respect to the scintillating crystal. A set of measurements were performed with the probe static inside the magnetic field (1 T), and a second set of measurements were performed moving the probe in and out of the magnet, in order to check the effect of a steep (more than 0.2 T/cm) magnetic field gradient. Figure 8 shows the average count rate in different conditions: a negligible variation simply due to counting statistics can be noticed.

Further tests were performed in the ATLAS and CMS experimental areas with a ^{60}Co source with a contact dose rate of 92 μSv/h, in different locations of the experimental halls, in the proximity

2019 JINST 14 T05007

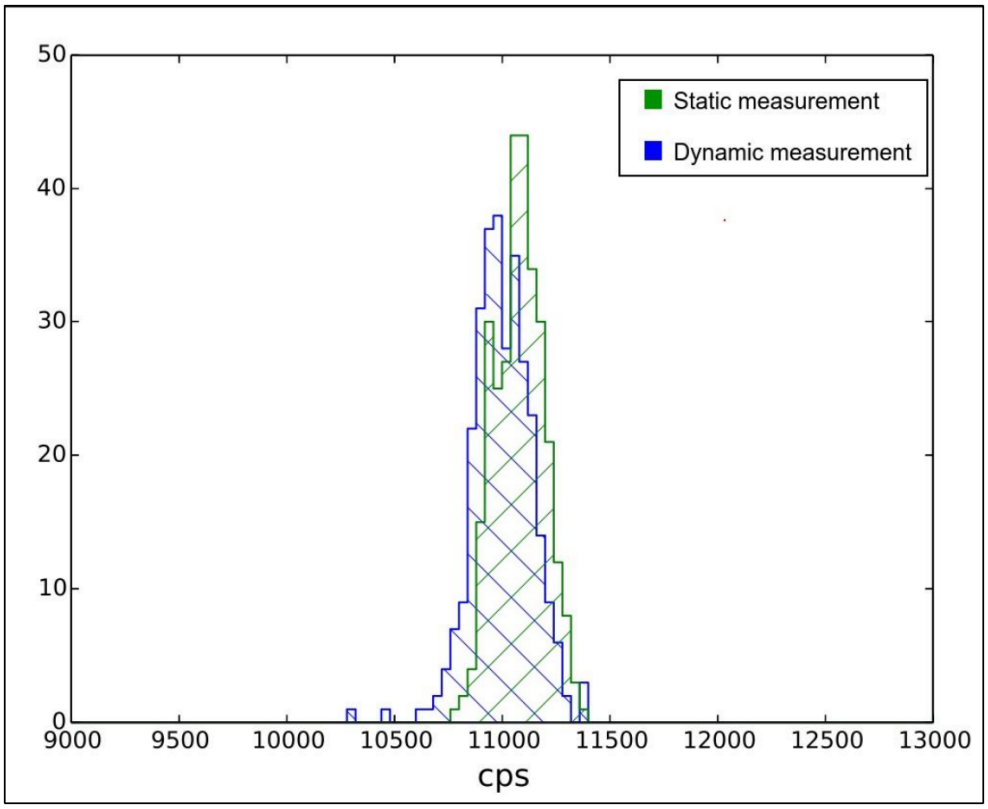

Figure 8. Comparison between dynamic and static measurements (300 s duration) in a 1 T magnetic field: a static measurement (green line) and a measurement acquired moving the detector in the field gradient (blue line).

of the detectors and inside ATLAS. The variation of the total integrated counts stayed within 2–3%. The highest field intensity reached in these tests was 1 T inside the ATLAS detector.

Finally, one of the final engineered version of the instrument (Unit 5) was tested in a 3 T magnetic field using the clinical MRI scanner at the university hospital in Lausanne (CHUV), using a ^{137}Cs source with a dose rate of 1.3 µSv/h at 10 cm. Both the active probe and the control unit were progressively slid into the bore of the MRI magnet and data were acquired during two minutes at each step. The magnetic field felt by the instrument was measured through a magnetometer attached to the probe and the mean value of the count rate distribution was calculated. As shown in figure 9 no remarkable differences can be noticed in the count rate by varying the magnetic field intensity. A measurement of the natural radiation background was also performed: the reduction in the count rate is due to the shielding effect of the MRI magnet on the probe while sliding it into the bore.

During all tests described above, a pulling force on the probe was felt starting from 0.3 T, which becomes intense above 1.5 T. This force is due to the eddy currents induced by the field gradient on the non-magnetic metallic components, mainly the aluminum box.

3.3 Temperature stability

Temperature tests were performed inside a climate chamber in the temperature range between −20°C and +50°C, in steps of 5°C and with an acquisition time of 2 h for each measurement point.

2019 JINST 14 T05007

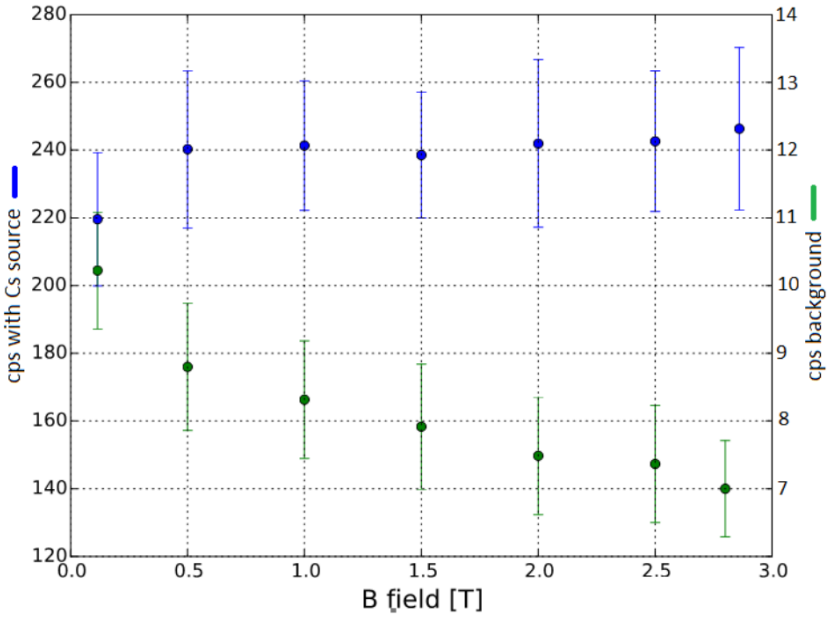

Figure 9. B-RAD count rate (cps) vs. magnetic field intensity in the presence of a ^{137}Cs source (blue) and background (green). Error bars indicate the FWHM of the count rate distribution.

The tests were performed on Unit 4 mounting a 1 inch NaI(Tl) crystal, and on Unit 5 mounting a $4 \times 4 \times 15\,\mathrm{mm}^3$ $LaBr_3$(Ce) crystal [6, 17]. Both the probe and the control unit were placed inside the chamber, with a ^{137}Cs source (1.3 µSv/h at 10 cm) positioned at a distance of about 3 cm from the crystal. The reference temperature was measured by a temperature sensor placed in the climate chamber close to the instrument. Figure 10 shows a clear variation of the response of Unit 4 as a function of temperature: the count rate decreases down to about 50% of the initial value with increasing temperature. The points that do not follow the general trend are due to wide and rapid temperature variations, typically those needed to bring the climate chamber back to 20°C before stopping the test, where the system could not thermalize as rapidly as the chamber. For temperature values between −20°C and 0°C the trend seems to flatten around 75 cps in the presence of the radioactive source. The background measurements in the temperature range between 0°C and 50°C are also presented in the graph, showing the same trend. The same measurements were taken with Unit 5 and the results are presented in figure 11. In this case the count rate decreases down to about 70% of the maximum value, due to the different crystal mounted inside the radiation probe ($LaBr_3$(Ce) instead of NaI(Tl)), which has a light yield with a lower temperature dependence.

The variable response of the detector as a function of temperature is mostly due to two overlapping effects: the variation of the crystal light yield and the variation of the breakdown voltage of the SiPM array. The latter, in particular, strongly affects the gain of the photodetector so that many of the signals coming from the crystal do not reach the comparator threshold anymore when the temperature increases. The drift in the breakdown voltage with the temperature variation of the SiPMs was measured and a coefficient of about 38 mV/°C was estimated (figure 12).

Various active (hardware) or passive (software) SiPM temperature response compensations have been studied and implemented in working devices nowadays [18, 19]. In our development a hardware solution was adopted to compensate this drift and to stabilize the SiPM gain in Unit 5.

2019 JINST 14 T05007

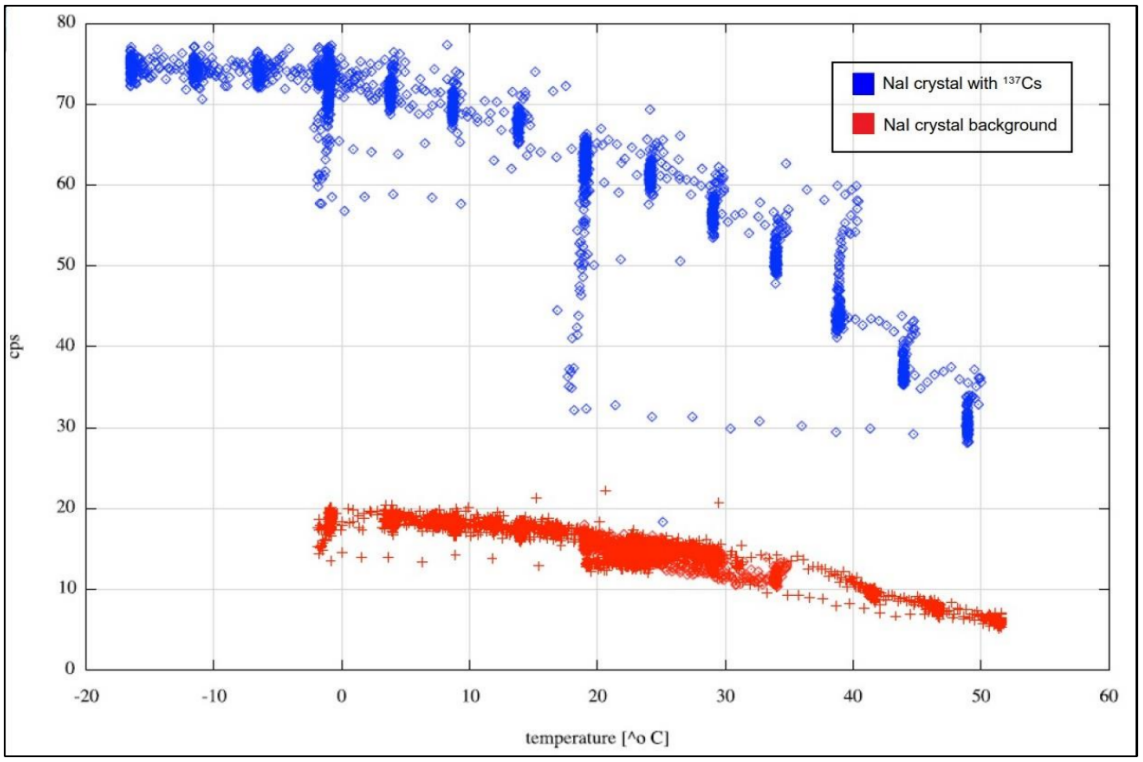

Figure 10. Count rate measurements with Unit 4 (NaI) as a function of the climate chamber temperature with a ^{137}Cs source (blue data) and without source (natural background, red data).

This solution is based on a current-controlled configuration called "current mirror". As shown in figure 13, the current in the temperature sensor, I_{temp1}, is driven by the resistor R47 connected to the temperature sensor and to the inverting input of the operational amplifier in the component LT6110. The slope of the temperature correction depends on this current, which can be regulated by modifying the value of R47. V_{fb} is the reference voltage of the linear regulator TPS7A4001, fixed at 1.17 V. The transfer function of this schematic is:

$$V_{out} = V_{DAC}\frac{R_{43}}{R_{43}+R_{42}}\left(-\frac{R_{39}}{R_{41}}\right) + V_{fb}\left(1+\frac{R_{39}}{R_{41}}\right) + I_{temp1}(T)\times R_{47} \tag{3.1}$$

where V_{DAC} is the voltage driven by a DAC placed in the control unit and V_{fb} is the voltage on the FB pin of the voltage regulator TPS7A4001.

Spectrometric tests were performed in the climate chamber using a ^{137}Cs source in order to check if the gain and consequently the position of the full energy peak changes as a function of temperature. This solution proved reliable and it was finally chosen to be integrated in both units. The results of the tests performed on Unit 4, mounting both a 1 inch × 1 inch NaI crystal and a 1 inch × 1 inch $LaBr_3$ crystal, are shown in figure 14 and figure 15. The position of the ^{137}Cs full energy peak as a function of temperature is now stabilized.

4 Energy response and spectrometric performance of the detector

In view of the design of the industrial version of the instrument, two further aspects were analysed: the energy response and the spectrometric performance of the $LaBr_3$ crystal coupled to the SiPM

2019 JINST 14 T05007

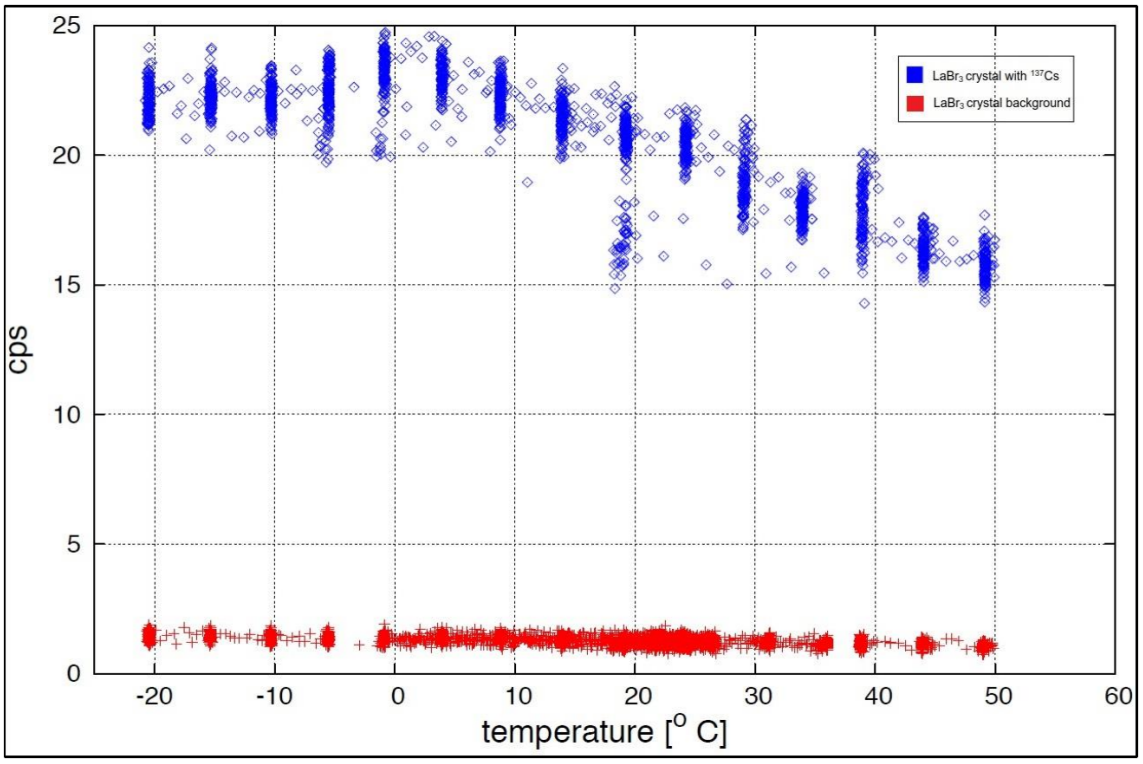

Figure 11. Count rate measurements with Unit 5 ($LaBr_3$) as a function of temperature with a ^{137}Cs source (blue data) and without source (natural and $LaBr_3$ internal background, red data).

array. A commercial instrument has to fulfil certain requirements in terms of both uniformity of its energy response and energy resolution for nuclide detection. It was preferred to perform this study on a system architecture similar to the final version. For the commercial version of B-RAD (see section 5) the choice of the crystal was made by taking into account the minimal volume required to discriminate weak radioactivity from background radiation. Tests of background discrimination were done with Units 1, 3, 4 and 5 by measuring the background radiation in a lead shielded chamber. These tests showed that the $10\,\emptyset \times 10\,mm^3$ cylindrical $LaBr_3$(Ce) crystal is large enough to detect natural background radiation with a reasonably short measurement time (10–20 seconds).

In order to match the size of one of the SiPM arrays available on the market, two samples of $15\,\emptyset \times 15\,mm^3$ cylindrical $LaBr_3$(Ce) crystals from different manufacturers where acquired and their performances compared in terms of internal background, energy threshold and energy resolution.

A 4×4 SiPM array from SensL (ArrayC-30035-16P) was investigated to check if it was a good alternative solution to the SiPMs by ST Microelectronics used in the prototype, which is not commercially available. The array is made up of sixteen $3 \times 3\,mm^2$ silicon elements with 4774 cells each of $35 \times 35\,\mu m^2$ size. The whole size of the array considering the external edges of each pixel is $16.8 \times 16.8\,mm^2$. A characterization study was performed on the SiPM array, showing a variation in the breakdown voltage between elements lower than 2% and a consequent high uniformity in the gain values.

2019 JINST 14 T05007

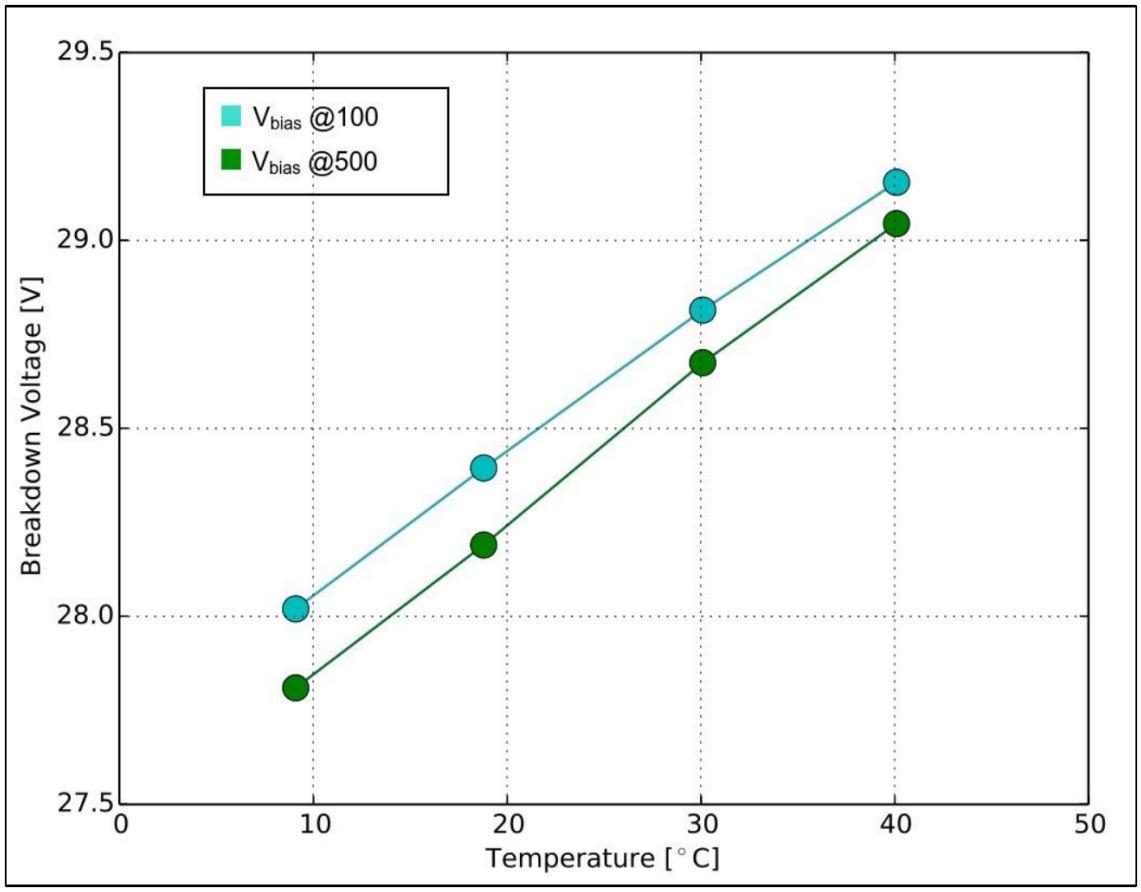

Figure 12. The breakdown voltage at each temperature is estimated through the I-V characterization curve of the ST SiPM. The value is defined as the point where the measured current is 100 (green line) or 500 (light blue line) times higher than the current estimated by the power fit on the first 10 V range.

4.1 Energy response

Radiation detectors intrinsically do not have a flat response as a function of energy and a correction is generally needed [20]. Usually, flattening of the energy response is achieved by adding physical filters (metallic foils of variable thickness attenuating the various photon energies selectively) [21], which cause a loss of sensitivity. Here we decided to follow a software approach as in [22].

The problem of obtaining a flat energy response in a dose rate measurement over the energy range from 60 keV to 1.3 MeV was studied using Geant4 Monte Carlo simulations for a cylindrical $15\,\emptyset \times 15\,\mathrm{mm}^3$ $LaBr_3$(Ce) crystal, but the results are easy to extend to different sizes and geometries. In terms of dose rate, the energy response of a cylindrical $LaBr_3$(Ce) crystal used as a counter is far from being flat. In general, the counting rate is a lot higher at lower energies, as expected from the definition of radiation dose as the amount of energy deposited per unit mass (the absorbed dose is measured in J/kg with special name Gray; radiation protection instrumentation are calibrated in the operational quantity ambient dose equivalent with special name Sievert, but for photons Gray and Sievert are numerically the same. The instrument measures counts, or count rate, that it is then converted into ambient dose equivalent via an appropriate built-in conversion factor). Following

2019 JINST 14 T05007

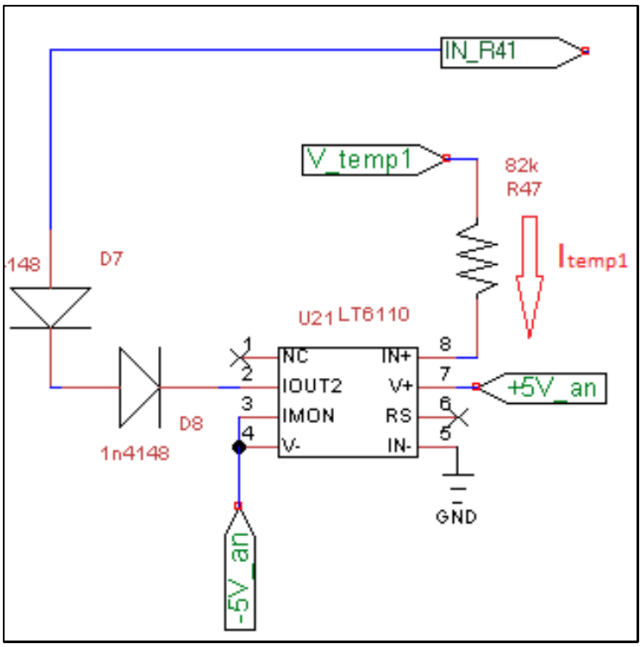

Figure 13. Schematic of the temperature compensation circuit mounted in Unit 5. The Vbias output is the result of the current nodal sum on R41. The current contributions come from the DAC output (V_{DAC}), the temperature sensor output (V_{temp1}) and the TPS7A4001 voltage regulator output (V_{fb}) shown in figure 5.

the Monte Carlo simulations, measurements were performed in order to confirm the computational results. The measurements were performed at the calibration laboratory of POLIMI with gamma sources and an X-ray generator, to study the B-RAD response as a function of mono-energetic (or nearly mono-energetic) photons. Three radioactive sources were used: ^{241}Am (60 keV), ^{137}Cs (662 keV) and ^{60}Co (1.17 MeV and 1.33 MeV). Eight energies from the X-ray generator were used (the spectra are shown in figure 16): S7 (48 keV), S8 (65 keV), S9 (83 keV), S10 (99 keV), S11 (116 keV), S12 (161 keV), S13 (220 keV) and S14 (249 keV).

Figure 17 shows the excellent agreement between Monte Carlo simulations and the experimental data, with a peak in the B-RAD sensitivity at around 80–90 keV and a nearly linear behaviour above approximately 300 keV. These preliminary studies were performed to provide ELSE NUCLEAR with quantitative results on the photon energy dependence and allow them to implement a software correction in the response of the commercial version of the instrument. As an example, figure 18 shows a simple software reweighting. The variation as a function of energy decreases from a factor of 20 to a completely flat response around one above 500 keV, with some variations around 15% concentrated in the low energy part of the spectrum, below 300 keV. The software compensation of the energy dependence in the example is achieved by normalizing the simulation results to the dose-to-flux conversion factors tables present in [23] and by exploiting the Geant4 response function of the detector, considering all shielding materials. This was done to provide the company with an example of unfolding algorithm compatible with the low power design of the instrument and able to flat the dose response with an acceptable uncertainty of maximum 15%.This has been implemented in the industrial version briefly described in section 5.

2019 JINST 14 T05007

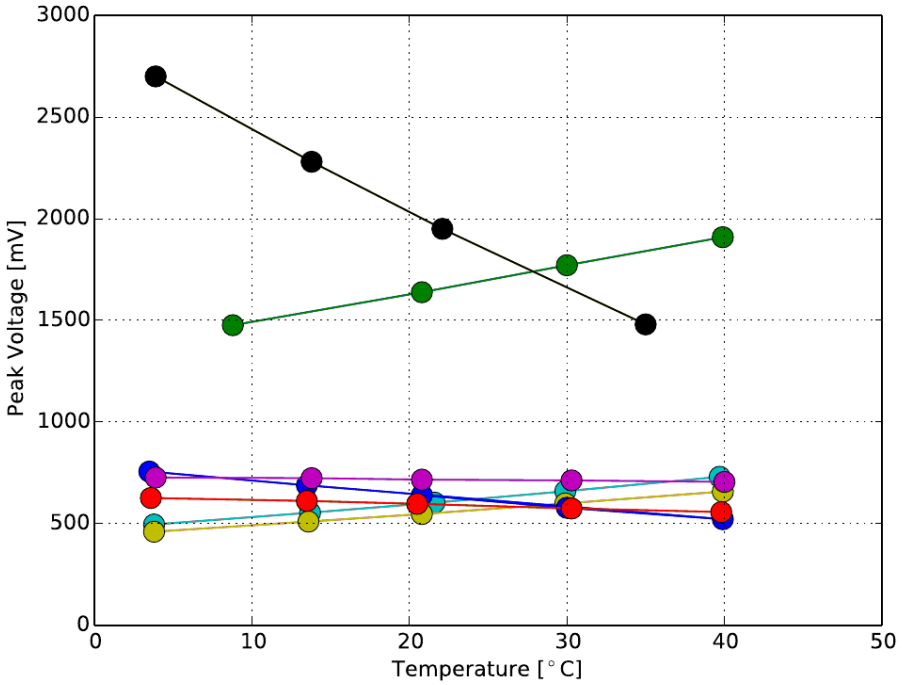

Figure 14. ^{137}Cs peak position as a function of temperature without (black curve, with slope −37.48 mV) and with compensation for different values of R47 for Unit 5. The tested values for R47 are 75 kΩ (green line, with slope 13.96 mV), 78.6 kΩ (light blue line, with slope 6.54 mV), 80.6 kΩ (yellow line, with slope 5.47 mV), 105 kΩ (violet line, with slope −0.606 mV), 114 kΩ (red line, with slope −1.975 mV), 150 kΩ (blue line, with slope −6.49 mV).

4.2 Spectrometric performances

Coupling the new SiPM array and the 15 Ø × 15 mm^3 $LaBr_3$ crystal previously chosen, spectra of ^{241}Am and ^{137}Cs sources were acquired to study the best expected energy resolution (figure 19) and the linearity of the system (figure 20). The output signals from the SiPM array is summed and sent to the acquisition electronics. The acquisition chain consisted in a NIM amplifier module (Silena Mod. 7613) [24] with a shaping time of 500 ns (unipolar output, gain ×20) and an Amptek MCA 8000D [25] for spectra acquisition and analysis. In this configuration, we obtained an energy resolution for the full energy peaks of ^{241}Am and ^{137}Cs of 19.2% and 6.8%, respectively. For the energy calibration we exploited the 33 keV x-rays emission of ^{137}Ba (FWHM = 30.3%) generated after ^{137}Cs decay.

5 The industrialised version by ELSE NUCLEAR

At the end of 2015 CERN granted a license on the B-RAD patent to the Italian company ELSE NUCLEAR. This allowed the company to start R&D activities to move the technology jointly developed by POLIMI and CERN from an advanced prototype level to an industrialised product to be commercialised worldwide. The main challenges encountered during this phase were: the development of a new electronics, which included the choice of new commercial passive and active components and the manufacturing of new printed circuit boards (PCBs) for both the control

2019 JINST 14 T05007

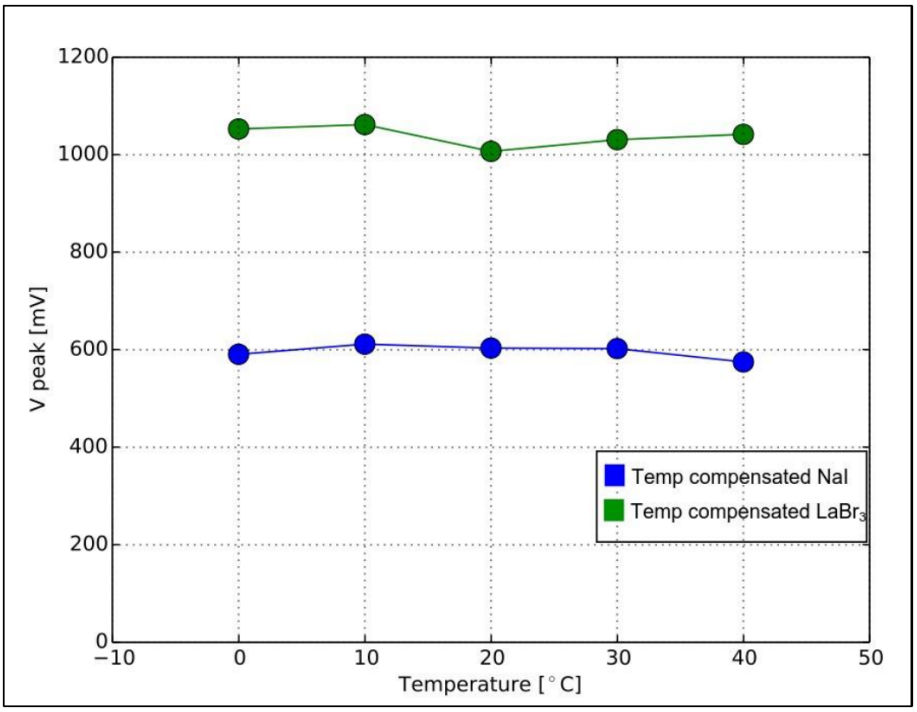

Figure 15. ^{137}Cs peak position as a function of temperature with compensation for R47 = 168 kΩ, comparing NaI (blue line) and $LaBr_3$ (green line) crystals in Unit 4.

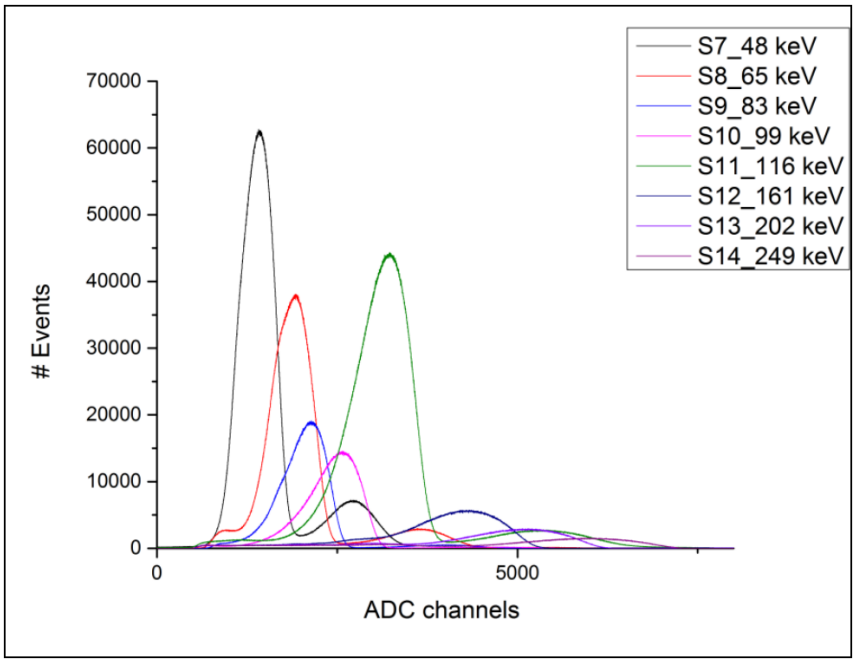

Figure 16. X-ray spectra generated by the tube, acquired with the 15 Ø × 15 mm^3 $LaBr_3$(Ce) crystal coupled to the SensL ArrayC-30035-16P.

2019 JINST 14 T05007

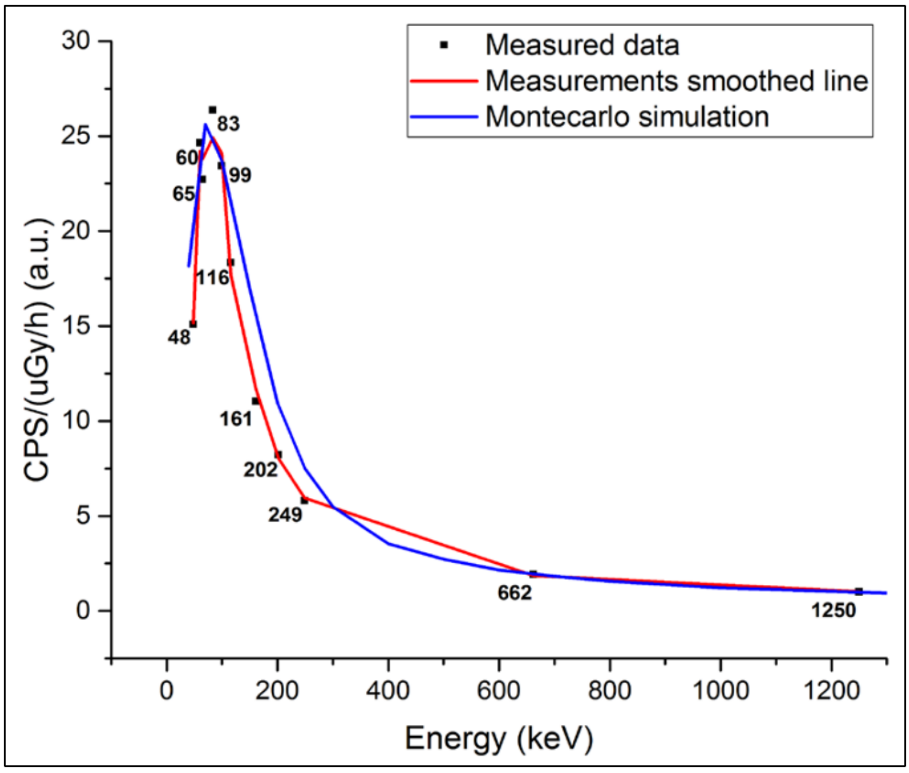

Figure 17. Comparison between Monte Carlo simulations (blue) and measurements performed with mono-energetic X-rays in the Calibration Laboratory of POLIMI.

unit and the active probe; the optimization of the crystal size, which in the standard version is $15\,\emptyset \times 15\,\mathrm{mm}^3$; the definition of new plastic/metallic materials for the control unit, in order to guarantee proper immunity from electromagnetic disturbances and induced current effects, by limiting at the same time the total detector weight and reduce the pulling force felt when operating in strong magnetic field; the implementation of a Hall probe for giving the end user an indication about the magnetic field intensity; the definition of a new, more ergonomic detector design; the choice of a new long-life battery. This last point proved to be particularly challenging, as recent severe regulations on the transport and use of Li-ion batteries in portable devices heavily reduced the range of available alternatives. This forced the company to design a customized battery pack sufficiently compact to be inserted in the B-RAD main unit, but lasting for more than 10 hours, in order to guarantee operation for a full working day. The commercial version of the B-RAD also implements a software with features typically needed by the end users during operation: possibility to visualize a spectrum in real time and to save it; log of all the alarm and malfunctioning events; a proprietary algorithm for radioisotope identification, already developed and tested by the company in the past in other crystal-based devices, which allows it operating as a spectroscopic personal radiation detector (SPRD).

The commercial version of the B-RAD was recently extensively tested at CERN in order to check its dose rate and spectrometric performances, the behaviour of the new battery and to verify the mechanical forces acting on the metallic components of the instrument. The measurements were performed inside a calibrated dipole magnet up to 1.5 T, increasing the magnetic field in 0.2 T

2019 JINST 14 T05007

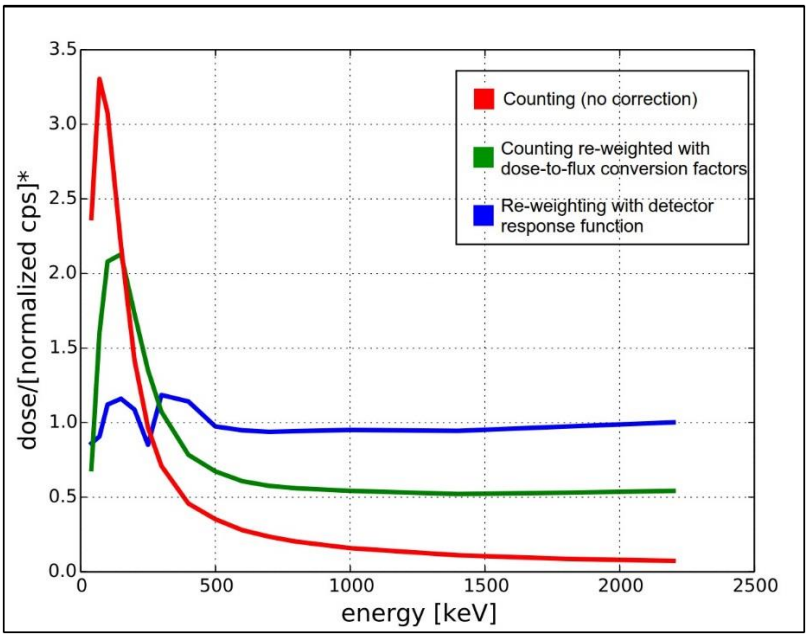

Figure 18. Main result of the Monte Carlo study: measured dose versus energy. The curves are all normalized using their mean over the energy range, i.e. a perfectly flat response would sit at 1. The red curve, showing the largest variation, is for a counting instrument (as in figure 17). The green curve combines counting function and the dose-to-flux conversion factors in [23]. The blue curve shows the result obtained reweighting the green curve with the response function of the detector. The maximum variation in this example is within 15%.

step; a ^{137}Cs source was fixed to the probe and both the count rate and the spectrum were acquired. The measurements were repeated for three different operating conditions: with only the main unit placed inside the dipole gap, with only the probe inside the dipole and with the entire B-RAD (main unit + probe) inside the dipole.

The battery operated correctly during all measurement cycles; both the LCD and LED displays worked properly. A pulling force was felt especially on the main unit, starting from 0.4 T, which becomes quite intense for values of magnetic field above 1 T. This is most likely at least partly due to the stainless steel screws, and the problem can be mitigated by replacing them with aluminium screws. The measured count rate remained constant for all values of the magnetic field and consistent with the value measured at 0 T (outside the dipole); a slightly deviation (less than 5%) from the reference value was noticed when measurements were performed after switching the detector off and then on again. The probe was tested in both static and dynamic conditions; a negligible variation only due to counting statistics was noticed. Eventually, with the unit placed inside the dipole the position of the ^{137}Cs peak in the acquired spectrum slightly shifts toward lower energy values with increasing magnetic field. This effect seems to be completely absent when only the probe is inside the dipole.

The final product is about to be made available commercially in several versions and will soon be delivered to customers active in both the research and the medical field. Figure 21 shows the commercial version of B-RAD equipped with a probe for both dose rate and gamma-spectrometry measurements.

2019 JINST 14 T05007

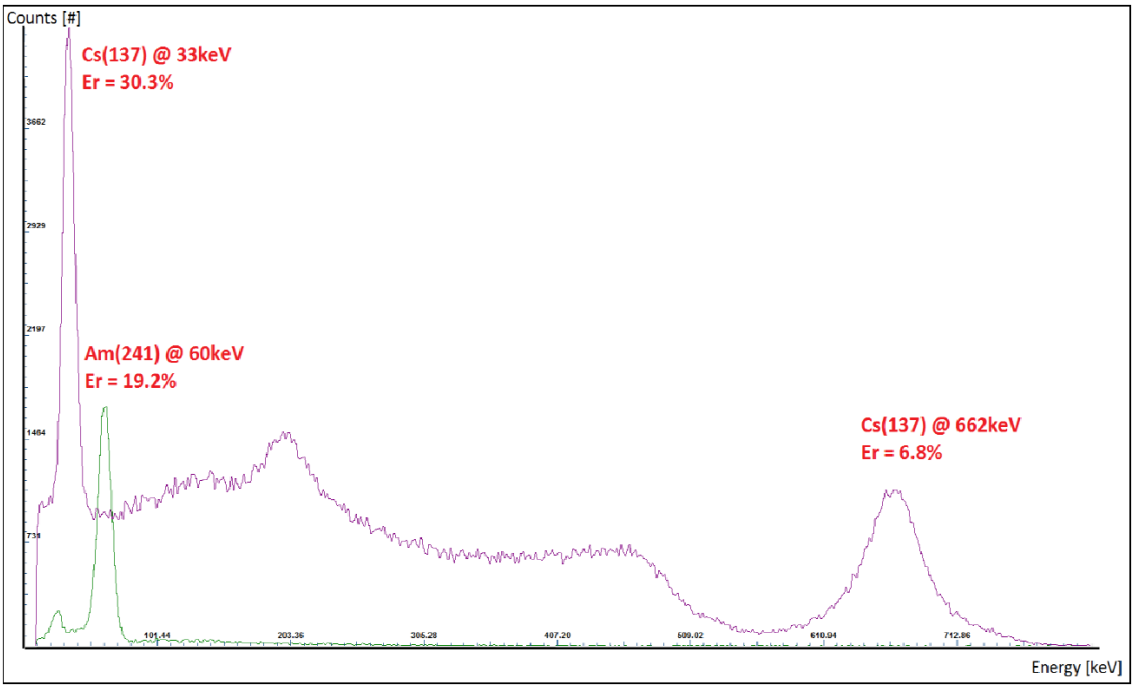

Figure 19. Spectra of ^{241}Am and ^{137}Cs source photons acquired with the SensL SiPM ArrayC-30035-16P and the EPIC [26] 15 ∅ × 15 mm^3 $LaBr_3$ crystal.

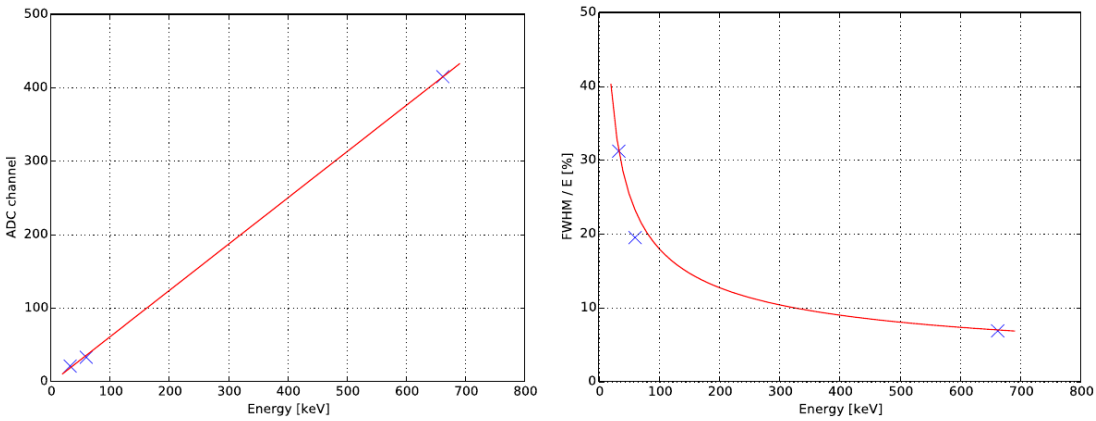

Figure 20. Linearity check of full energy peak channel position as a function of energy (33 keV, 60 keV, 662 keV) on the left and FWHM/E_{peak} as a function of the energy on the right.

6 Conclusions

A novel radiation survey meter employing a $LaBr_3$(Ce) scintillating crystal coupled to a matrix of SiPM was developed for operational radiation protection measurements in the presence of intense magnetic fields. The performance of the instrument in terms of linearity of its response and measurement of ambient dose equivalent rate were confirmed with extensive tests in a calibrated dipole magnet and in 3 T MRI scanner, as well as in operational conditions in the ATLAS and CMS experimental areas at CERN. The instrument proved to operate correctly in both static and dynamic

2019 JINST 14 T05007

Figure 21. The commercial version of the B-RAD by ELSE NUCLEAR. The probe can also be mounted on an extension rod for measurements at a distance.

conditions. After the development of the first prototype, five engineered units of B-RAD were built, three used for routine measurements at CERN, the others employed for R&D towards a commercial version of the instrument.

In order to stabilise the B-RAD response versus temperature, a circuit implemented in the probe allows the bias voltage to follow the drift of the SiPM breakdown voltage so as to keep the overvoltage and the SiPM gain constant. In this way, the measured count rate is not influenced by variations in the ambient temperature over a broad range.

By combining counting, energy measurements and an ad hoc reweighting scheme, it is possible to obtain a flat energy response in dose rate with the given detector without resorting to physical filters. This solution has been implemented in the commercial version of the instrument. The procedure has been devised and validated using Monte Carlo simulations, well reproducing the experimental response of the $LaBr_3$(Ce) crystal.

Spectrometric measurements were performed in order to check the best expected performance of the final set-up (a $15\,\emptyset \times 15\,mm^3$ cylindrical $LaBr_3$(Ce) crystal coupled to the SensL ArrayC-30035-16P), achieving an energy resolution of 6.8% at 662 keV with a lower energy threshold below 33 keV.

B-RAD has been licensed to ELSE NUCLEAR, which has produced a commercial version. In parallel, the development of three additional probes is being pursued at CERN, to be coupled to the B-RAD central unit in order to exploit the same central electronics for signal processing: a surface contamination probe, an air contamination probe and a neutron dose rate/spectrometry probe, all based on coupling a scintillating crystal with a SiPM array.

Apart for its use at CERN, B-RAD has various potential fields of applications such as measurements of residual radioactivity on activated accelerator components, radiation surveys of permanent magnets or activated magnets with a residual magnetic field, surveys around electron linear accelerators for industrial applications and in the medical environment, e.g. surveys around PET/MRI

2019 JINST 14 T05007

scanners and at the latest generation of medical electron linacs coupled to an MRI for image-guided radiation therapy. More generally, the technological solutions implemented and tested for B-RAD are useful for radiation monitoring in processes requiring the presence of magnetic fields, e.g. scrap metal handling or handling of containers using lifting magnets

Acknowledgments

We wish to thank prof. M. Caresana (POLIMI) for helping with the measurements at the Calibration Laboratory of the Polytechnic of Milan, C. Pirovano (POLIMI) for technical assistance, S. Emami for developing the C language version of the firmware, M. Buzio and X. Gontero (CERN) for putting at our disposal the dipole magnet for the tests in magnetic field, I. Brunner, F. Ferrulli and L. Gallego Manzano (CERN) for helping with the test with the dipole and in ATLAS and CMS, J. Damet of the Institut de Radiophysique in Lausanne, J. Yerly, N. Cherbuin and M. Stuber at CHUV (the Lausanne university hospital) for making available the MRI scanner for the test at 3 T field and for assisting us during the measurements, G. Manessi (ELSE NUCLEAR) for the description of the commercial version of B-RAD.

References

[1] https://home.cern/fr/about/experiments.

[2] https://www.dhs.gov/sites/default/files/NUSTL-SAVER_PRD-SPRD-MSR_1707-508.pdf.

[3] R.H. Thomas and G.R. Stevenson, *Radiological safety aspects of the operation of proton accelerators*, IAEA Technical Reports Series, volume 283, IAEA, Vienna Austria (1988) [IAEA-TR-283] [STI-DOC-10-283] [STI-DOC-010-283].

[4] A. Fazzi and M. Silari, *Portable Radiation Detection Device for Operation in Intense Magnetic Fields*, U.S. Patent 20170199284A1 (2017).

[5] http://www.elsenuclear.com/en/.

[6] Saint-Gobain, *Lanthanum Bromide Material Datasheet*, (2019) https://www.crystals.saint-gobain.com/products/brillance-labr3-lanthanum-bromide.

[7] D.K. Panda, Y.B. Acharya, S.K. Goyal and D. Benerjee, *Characterization of lanthanum bromide scintillator for gamma ray spectroscopy*, in proceedings of the *SAMTI-2011: Symposium on Advanced Measurement Techniques and Instrumentation*, Mumbai, India, 2–4 February 2011.

[8] Microchip, *PICDEM PIC18 Explorer Demonstration board user's guide*, Microchip Technology Inc. (2008).

[9] M. Mascotto, *Silicon Photomultiplier Technology at STMicroelectronics*, (2011) https://indico.cern.ch/event/117424/contributions/1329247/attachments/56777/81753/STMicroelectronics_SIPM_CERN_2011-02-17.pdf.

[10] http://www.sensl.com/downloads/ds/UM-ArraySMT.pdf.

[11] https://www.ti.com/lit/ds/symlink/sn74ac04.pdf.

[12] https://www.vishay.com/docs/71133/si4532ady.pdf.

2019 JINST 14 T05007

[13] D.F. Spencer, R. Aryaeinejad and E. Reber, *Using the Cockroft-Walton voltage multiplier design in handheld devices*, in proceedings of the *2001 IEEE Nuclear Science Symposium Conference Record (Cat. No.01CH37310)*, San Diego, CA, U.S.A., 4–10 November 2001, IEEE (2002), pp. 746–749.

[14] http://www.ti.com/lit/ds/symlink/tps7a4001.pdf.

[15] G.F. Knoll, *Radiation Detection and Measurements*, 4th edition, John Wiley & Sons Inc. (2010).

[16] M. Brugger, P. Carbonez, F. Pozzi, M. Silari and H. Vincke, *New radiation protection calibration facility at CERN*, *Radiat. Prot. Dosim.* **161** (2014) 181.

[17] Saint-Gobain, *Sodium Iodide Material Datasheet*, (2019) https://www.crystals.saint-gobain.com/products/nai-sodium-iodide.

[18] F. Licciulli and C. Marzocca, *An active compensation system for the temperature dependence of SiPM gain*, *IEEE Trans. Nucl. Sci.* **62** (2015) 228.

[19] M. Baszczyk, P. Dorosz, S. Głąb, W. Kucewicz, Ł. Mik and M. Sapor, *Silicon photomultiplier gain compensation algorithm in multidetector measurements*, *Metrol. Meas. Syst.* **20** (2013) 655.

[20] A.S. Pradhan, *Photon Energy Response of Luminescence Dosemeters and its Impact on Assessment of $H_p(10)$ and $H_p(0.07)$ in Mixed Fields of Varying Energies of Photons and Beta Radiation*, *Radiat. Prot. Dosim.* **101** (2002) 173.

[21] A.S. Pradhan and R. Bhatt, *Metal filters for the compensation of photon energy dependence of the response of CaSO4:Dy — Teflon TLD discs*, *Nucl. Instrum. Methods* **166** (1979) 497.

[22] Y. Knafo et al., *Flattening the Energy Response of a Scintillator Based Gamma Dose Rate Meter Coupled to SiPM*, in proceedings of the *Conference of the Nuclear Societies in Israel*, Dead Sea, Israel, 11–13 February 2014.

[23] S.G. Kwon, C.W. Ha, P.S. Moon, K.E. Kim and C.C. Yook, *Calculation of neutron and gamma-ray flux-to-dose-rate conversion factors*, *J. Korean Nucl. Soc.* **12** (1980) 171.

[24] http://www.geocities.ws/silena_spa/silena/products/nimamps/7613p.htm.

[25] http://amptek.com/wp-content/uploads/2016/06/MCA-8000D-Digital-Multichannel-Analyzer-Specifications.pdf.

[26] http://www.epic-scintillator.com/LaBr-crystal-scintillator/LaBr3-Scintillator-15x15mm.

2019 JINST 14 T05007